communications physics

ARTICLE

https://doi.org/10.1038/s42005-023-01135-x OPEN

A multi-MeV alpha particle source via proton-boron fusion driven by a 10-GW tabletop laser

Valeriia Istokskaia[1,2✉], Marco Tosca[1,3,4], Lorenzo Giuffrida[1], Jan Psikal[1,2], Filip Grepl[1,2], Vasiliki Kantarelou[1], Stanislav Stancek[1,5], Sabrina Di Siena[6], Arsenios Hadjikyriacou[1,2], Aodhan McIlvenny[7], Yoann Levy[8], Jaroslav Huynh[8], Martin Cimrman[2,8], Pavel Pleskunov[3], Daniil Nikitin[3], Andrei Choukourov[3], Fabio Belloni[9], Antonino Picciotto[10], Satyabrata Kar[7], Marco Borghesi[7], Antonio Lucianetti[8], Tomas Mocek[8] & Daniele Margarone[7,1✉]

Nuclear fusion between protons and boron-11 nuclei has undergone a revival of interest thanks to the rapid progress in pulsed laser technology. Potential applications of such reaction range from controlled nuclear fusion to radiobiology and cancer therapy. A laser-driven fusion approach consists in the interaction of high-power, high-intensity pulses with H- and B-rich targets. We report on an experiment exploiting proton-boron fusion in CN-BN targets to obtain high-energy alpha particle beams (up to 5 MeV) using a very compact approach and a tabletop laser system with a peak power of ~10 GW, which can operate at high-repetition rate (up to 1 kHz). The secondary resonance in the cross section of proton-boron fusion (~150 keV in the center-of-mass frame) is exploited using a laser-based approach. The generated alpha particles are characterized in terms of energy, flux, and angular distribution using solid-state nuclear-track detectors, demonstrating a flux of ~10^5 particles per second at 10 Hz, and ~10^6 per second at 1 kHz. Hydrodynamic and particle-in-cell numerical simulations support our experimental findings. Potential impact of our approach on future spread of ultra-compact, multi-MeV alpha particle sources driven by moderate intensity (10^{16}-10^{17} W/cm^2) laser pulses is anticipated.

[1] ELI Beamlines Facility, The Extreme Light Infrastructure ERIC, Dolni Brezany, Czech Republic. [2] Czech Technical University in Prague, Faculty of Nuclear Sciences and Physical Engineering, Prague, Czech Republic. [3] Charles University, Faculty of Mathematics and Physics, Department of Macromolecular Physics, Prague, Czech Republic. [4] MARVEL FUSION GmbH, Munich, Germany. [5] Palacký University in Olomouc, Faculty of Science, Joint Laboratory of Optics of Palacký University and Institute of Physics of the Czech Academy of Sciences, Olomouc, Czech Republic. [6] Physics Department, University of Naples Federico II, Naples, Italy. [7] Centre for Light-Matter Interactions, School of Mathematics and Physics, Queen's University Belfast, Belfast, United Kingdom. [8] HiLASE Centre, Institute of Physics (FZU), Czech Academy of Sciences, Dolni Brezany, Czech Republic. [9] School of Electrical Engineering and Telecommunications, Faculty of Engineering, UNSW Sydney, Sydney, Australia. [10] Micro-Nano Facility - Sensors and Devices Center, Fondazione Bruno Kessler (FBK), Trento, Italy. ✉email: valeriia.istokskaia@eli-beams.eu; daniele.margarone@eli-beams.eu

The nuclear reaction between protons and boron ions is one of the most prominent in the context of advanced fusion schemes. In the past years, the reaction has been extensively studied[1–6] and nowadays is referred to as proton-Boron (pB) fusion: it engages boron-11 isotope at the input and results in the production of three energetic alpha particles at the output ($^{11}B(p,\alpha)2\alpha$). According to previous studies[7–9], the reaction cross section shows two peaks at low energy (in the center-of-mass frame, CoM)—the broad main resonance at 612 keV (1.2 barn) and the narrow secondary one at 148 keV (0.1 barn). The resulting alpha particles energy spectrum is strongly peaked at ~4 MeV, spanning over a large energy range (up to ~7 MeV in the laboratory)[10,11].

The interest of such fusion reaction lies in its aneutronic nature (<1% of the energy irradiated in neutrons at CoM energies >2.8 MeV[12]) and high yield of charged alpha particles. Apart from being an attractive candidate for controlled nuclear fusion energy generation (combination of "ultraclean" operation, readily available fuel, and advantageous electricity conversion[3,13–15]), the pB fusion could also be exploited as a valuable high-brilliance secondary source of alpha particles for multidisciplinary applications using compact and cost-effective approaches. For instance, much effort has been recently put into investigation[16,17] and pre-clinical tests[18,19] of the so-called Proton-Boron Capture Therapy (PBCT)—an enhancement of the proton therapy biological effectiveness based on the pB reaction, where a boron solution is potentially injected into deep-seated tumors prior to the irradiation with clinical proton beams. Moreover, gamma radiation emitted at the same time can be exploited for online imaging and dose monitoring during tumor treatment[20,21]. Another promising potential application of alpha particle sources is medical radioisotopes production for imaging, therapy, or theranostics[22,23].

Since the beginning of 2000s, a renewed interest in pB fusion has arisen thanks to advancements in laser technology. Exploiting short-pulse, high-power lasers leads to plasma conditions far from thermodynamic equilibrium, hence very different from conventional inertial confinement fusion schemes[3,4,14]. After the first experiment on laser-driven pB fusion[24], steady progress in the emitted alpha yield has been reported in multiple works based on a beam-plasma approach (using either the "in-target" or the "pitcher-catcher" scheme), as summarized in reference[11]. Different laser regimes (intensity, pulse duration, etc.) and target composition have been explored[11,25–29]. However, only the main resonance in the cross-section of such fusion reaction (~610 keV, CoM) was used, while the secondary resonance (~150 keV, CoM) remained unexplored thus far.

In this work, we describe an experimental investigation using the PERLA B laser available at the HiLASE Center[30], which is an ultra-compact 10-GW laser system delivering ~1.5-ps pulses at high-repetition rate (up to 1 kHz) to take advantage of the secondary resonance of p-B fusion. Our findings pave the way towards the optimization of a tabletop source of energetic (up to 5 MeV) alpha particles through the exploitation of laser-driven p-B nuclear fusion.

Results

Experimental setup. In order to accelerate protons up to the energies covering the secondary resonance energy peak required for p-B fusion (148 keV), the tabletop PERLA B laser system was used[31]. The main laser pulse was preceded by a ~1.5-ps prepulse (with intensity contrast ratio of $\sim 10^{-3}$) generating a long preplasma plume (~30 μm) at the target front side that allowed to enhance the subsequent proton acceleration in the backward direction[31]. Figure 1a shows the arrangement of laser, target, and detectors inside the vacuum chamber, while Fig. 1b reports the post-processed laser profile at the focal plane, showing an average laser intensity of $\sim 2 \times 10^{16}$ W/cm^2 achieved by focusing the laser beam down to a diameter of ~2.6 μm (FWHM). Further details are described in the section Methods.

In this experiment, the "in-target" fusion scheme[11] was employed, i.e., the reaction was triggered inside the target volume which contained both protons and boron atoms in a two-layer geometry. A 3-mm thick boron nitride (BN) substrate served as a source of boron ions for the fusion reaction. A 600-nm thick hydrocarbon plasma polymer film was deposited on it (see Methods) and provided protons for acceleration in the laser-driven quasistatic electric field[32] with energies sufficient to cover the secondary resonance in the p-B fusion cross-section (~300 keV cutoff, see Fig. 4c). The use of a solvent-free method of plasma polymerization was motivated by environmental concerns. Hereafter we refer to the target as CH-BN.

Long stripes of CR39 nuclear-track detectors provided an estimation of the alpha particle flux based on the number of tracks recorded by such passive diagnostics. The stripes were positioned in front of the target and accumulated the imprints of alpha particles generated in several hundreds of shots under the same experimental conditions with the goal of maximizing the signal-to-noise ratio. The stripes of CR39 were divided into two groups (blank and covered with Al filter of 2.4 μm thickness) and were irradiated simultaneously. To monitor the ion signal online and thus be able to adjust the laser-plasma parameters to maximize it, a Faraday Cup (FC) was used as a supplementary diagnostic. However, the sensitivity of FC was not sufficient for detecting the protons with the highest energy (hence a relatively low charge) on a shot-to-shot basis. The FC however provided valuable information on the low-energy particle distribution, helping to optimize the interaction.

Measurements of alpha particles generated in laser-plasma interaction. According to experimental studies[33–35], emission of laser-accelerated protons and heavier ions under the given experimental conditions (backwards acceleration from a thick target using a ps-long pulse) is mainly directed along the target normal with divergence ~30°. On the contrary, alpha particles are expected to undergo different angular distribution and reach the detector even at large angles, since they are produced via a different mechanism (nuclear fusion reaction in the laser-generated plasma) and emitted in 4π steradian solid angle in the CoM frame. Therefore, the CR39 stripes were extended to cover also large angles with respect to the target normal (from −10° up to 48°, which was the limit due to geometrical reasons). Filtering with 2.4-μm thick Al foils (used on some part of the CR39) enabled distinguishing the alpha particle tracks from the mixture of low-energy protons and ions. According to ion-stopping power calculations, the Al filter cuts the vast majority of the emitted particles remaining "transparent" only to high-energy fusion-produced alpha particles ($E > 680$ keV) and high-energy protons (>250 keV).

A total number of 670 shots were done on a single CH-BN target (~6 × 4 cm^2) during one shooting series; every shot was fired onto a fresh surface. Figure 2a shows an image of particle tracks recorded by a segment of the CR39 sample in the filtered region at a large angle from the target normal (39°) after 3 h of etching in NaOH solution (see Methods). For comparison, a sample of the unfiltered CR39 region located at the target normal is shown in Fig. 2b.

For verification of the results, CR39 samples were exposed to laser irradiation under the same conditions also with a reference poly(methyl methacrylate) (PMMA) target installed. Since boron was absent in the reference target, alpha particles were not

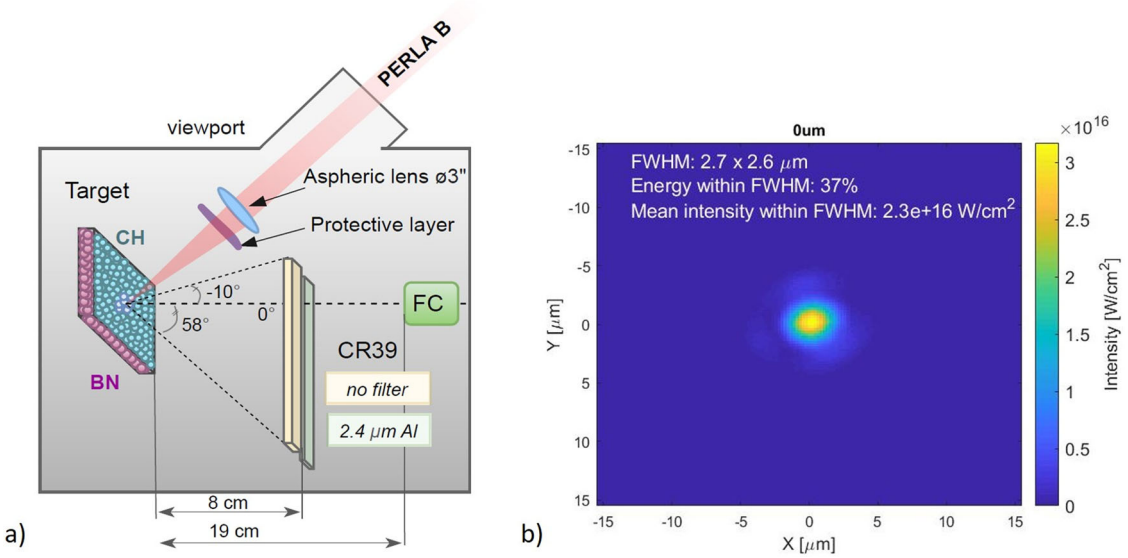

Fig. 1 Schematic of the experimental setup and laser focal spot profile measurement. a Experimental setup inside the vacuum chamber: the laser pulse is incident on the CH-BN target (containing protons and Boron) at 45° through a viewport and is focused by an aspheric lens located inside the chamber. The lens is protected from debris by a transparent protective glass. Two CR39 stripes with plain and filtered regions are aligned in front of the target, leaving the equatorial plane unobstructed for the FC (Faraday Cup) placed at the target normal. **b** Post-processed photo of the spatial-intensity profile of the laser focal spot measured on target. The FWHM (full width at half maximum) size of the focal spot along with the laser energy and mean intensity encircled inside it are stated in the figure.

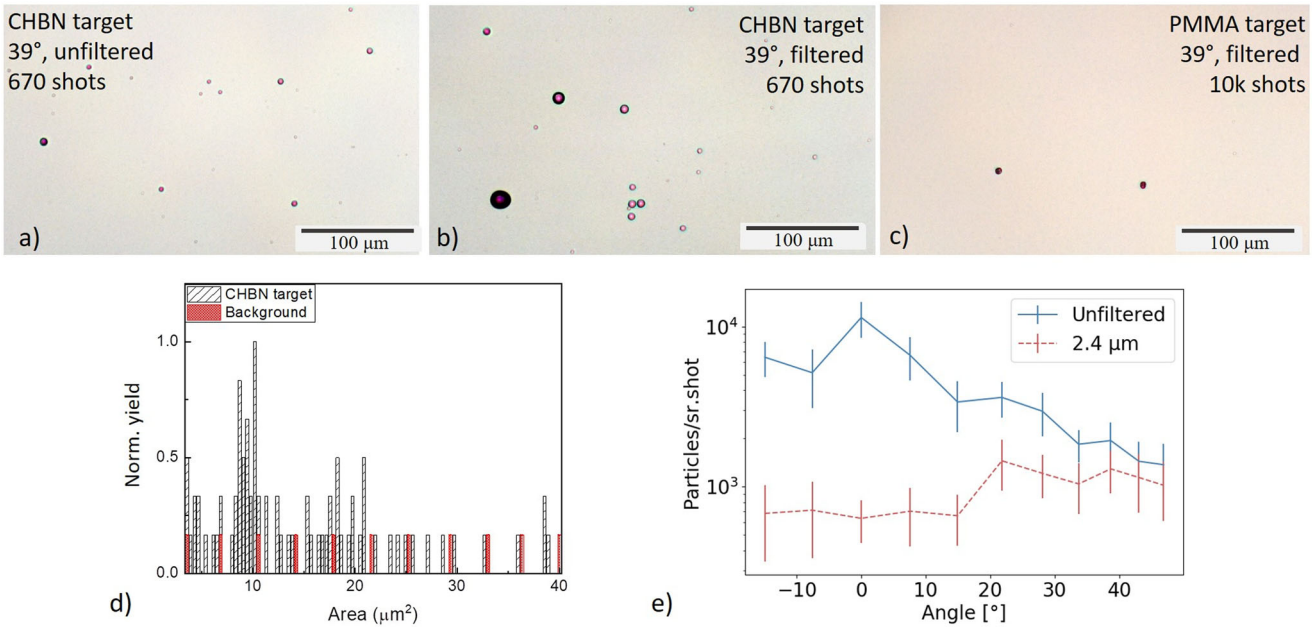

Fig. 2 CR39 measurements and results. a Example of the unfiltered CR39 region at 0° in the case of CH-BN target after 3 h of etching, showing tracks from various particles emitted from plasma. The total number of accumulated shots is 670. **b** Example of the irradiated CR39 detector located at 39° and filtered by a 2.4-μm thick Al foil in the case of CH-BN target after 3 h of etching. All the dots are ascribable to alpha particles of different energies (larger dots correspond to low-energy alpha particle loosing most of their energy in the Al filter). **c** Example of the CR39 detector irradiated and etched under similar conditions as in a) in the case of reference PMMA (polymethyl methacrylate) target (no boron content). The total number of shots on the target was 10^4. The two tracks visible in the image are within the background level. **d** Histogram showing the area distribution of the detected particle tracks for all the CR39 samples under conditions described in **a**). The background influence is highlighted in red and is considered as 10 particles per statistics. **e** Angular distribution comparison of particles detected by CR39 in the unfiltered (blue solid line) and filtered (red dashed line) regions. The error bars are given by the standard deviation error. The background (80 particles/sr/shot) is already subtracted from the data.

expected in this test. It is worth noting, that the total number of shots, in this case, was kept more than ten times higher in comparison with the CH-BN target in order to enhance the detection probability, i.e., the number of high-energy protons passing the filter under high irradiation flux. A filtered segment of the reference CR39 at the same angle (39°) is presented in Fig. 2c) showing only a few dots in the image, which is comparable to the natural background level (observed on unexposed CR39 samples).

The total track area distribution corresponding to the measurement described in Fig. 2a is shown in Fig. 2d: the majority of particle track areas falls within a range of 10 μm^2–20 μm^2.

The angular distribution of the measured particles was reconstructed for both filtered and unfiltered CR39 stripes and is shown in Fig. 2e. It is evident that for large angles (>33°) the filtered and unfiltered curves coalesce within the error bars, showing ~1000 particles/sr/shot.

Therefore, a combination of filtering and large-angle detector location excludes the presence of plasma ions on the CR39 and allows one to assume that the recorded tracks are generated by the alpha particles produced in the nuclear fusion reaction. Moreover, an increase at around 22° present for both cases might indicate that the alpha emission is shifted from the target normal towards larger angles while the abundance of laser-accelerated ions decreases with increasing angle. This trend is in agreement with experimental findings presented in our previous work[27], where the reduction of alpha particles at small angles was explained by scattering and/or absorption by the plasma plume.

Reconstruction of energy distribution and total number of alpha particles. Based on the CR39 measurements described above, we assumed that the tracks recorded on the stripes at large angles are produced exclusively by alpha particles after subtraction of the natural background. The track area distribution was converted into alpha particle energy spectrum by means of a calibration curve. The results for the largest angles (39°, 43°, and 48°) were summed up and interpolated. Figure 3 shows the resulting energy distribution of alpha particles. The energies are in the range of 1–4.5 MeV and peaked at ~3.5 MeV.

Although such energy distribution is in general agreement with the previous theoretical and experimental findings[10,11,27,29], the strongest peak is slightly shifted towards lower energies. We attribute this effect to collisional energy losses of the alpha particles in the dense pre-plasma plume.

The total number of measured alpha particles was calculated from the angular distribution (filtered case) shown in Fig. 2e. By integrating the measured curve, it is possible to obtain a resulting alpha particle yield of 9684 ± 905 alpha particles/sr/shot. Based on our experimental data, it is not possible to provide an accurate estimation of the total alpha particle yield emitted in the backward direction from the target unlike usually done in experiments performed at conventional accelerators, where a theoretical fit can be easily applied[36]. Thus, the total angular distribution of the alpha particles produced in a laser-driven pB fusion reaction is yet to be properly characterized.

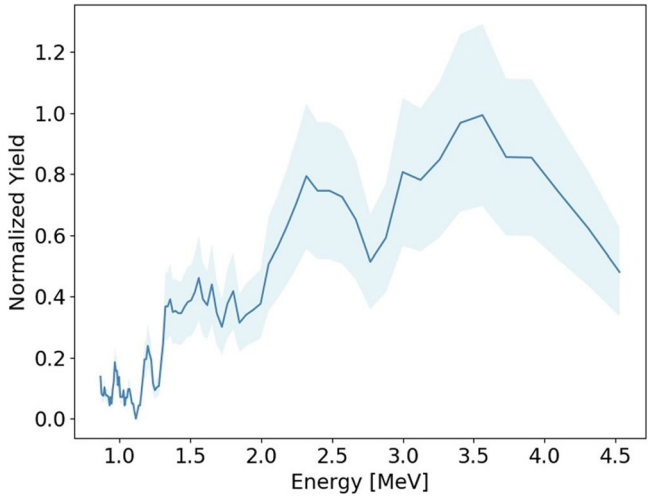

Fig. 3 Alpha particles energy distribution. Alpha particle energy distribution was obtained by conversion of the area distribution for filtered regions of CR39 at large angles (>39°) using a calibration curve. The shaded region on the plot represents the experimental uncertainties estimated ~30% of the measured values.

Hydrodynamic (HD) and particle-in-cell (PIC) simulation results. To investigate the underlying physics, two different simulation approaches were combined and the results are shown in Fig. 4. In the first step, HD simulations were performed using the 2D cylindrical FLASH[37,38] code in order to simulate the interaction of the focused prepulse with the target. The laser prepulse intensity contrast was set to be ~10^{-3}, i.e., the prepulse carried a significant fraction of the main pulse energy thus leading to the formation of a large cloud of preplasma prior to the arrival of the main pulse. The outcome of the HD simulations adjusted for the input of the PIC simulations is shown in Fig. 4a: as it can be seen, due to the prepulse interaction with the target, the preplasma expanded to ~30 μm just before the arrival of the main pulse. The corresponding mean density of the Boron ions in the preplasma was ~5×10^{19}/cm^3. In the second step of the simulation study, the HD density output was used as a PIC input in order to model the interplay between the main pulse and the target preplasma since, at this intensity, the hydrodynamic assumption begins to breakdown where the electron distribution is no longer Maxwellian and the timescales of the physics becomes shorter than the hydrodynamic timescales. According to the PIC results, the main bulk of the preplasma formed by the time of the main pulse arrival was overdense (opaque to the laser radiation) with electron density reaching up to $10 \times n_{ec}$, where n_{ec} is the critical density. Therefore, the laser pulse was prevented from propagating into this preplasma region and from reaching the initial target surface due to its reflection from the preplasma. Figure 4b illustrates this process at 1500 fs after the pulse entered the simulated region. The main interaction happened at a distance of ~20 μm from the target surface, where the electron density starts to be equal to the critical density.

To estimate the probability of the fusion reaction, energies of laser-accelerated protons were monitored during PIC simulations in the forward and backward directions with respect to the target. Protons crossing the simulation border behind the target original area were recorded as moving in the forward direction, while the ones still located in the simulated region at the end of the simulation (3.5 ps) were considered as "backward". The energy distribution for both proton groups is shown in Fig. 4c. Protons moving towards the target interior show maximum energies of only 30 keV, while protons moving backwards are accelerated to substantially higher energies, up to 300 keV, thus widely covering the secondary resonance peak of the p-B fusion cross-section (0.1 b). This implies that under the explored experimental conditions the most efficient proton acceleration occurred mainly backwards (direction opposite to the laser propagation), while protons accelerated forwards (into the target) did not contribute to the generation of alpha particles via pB fusion since the reaction rate is negligible for proton energies below 100 keV (steep drop in the reaction cross-section). Therefore, pB fusion reactions occurred in the boron plasma cloud (assuming boron at rest) created by the laser prepulse rather than in the target region.

High-repetition-rate operation at 1 kHz. Since the PERLA laser system is capable of 1 kHz operation regime, a constant source of alpha particles is potentially reachable under the described

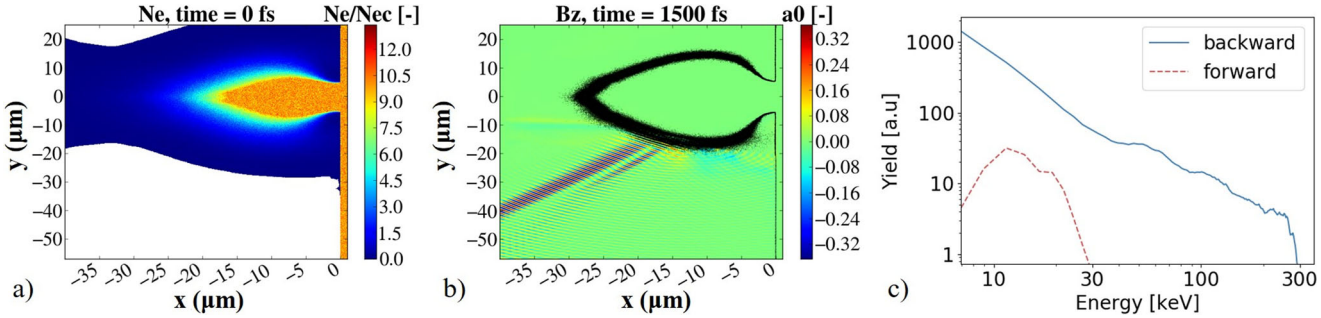

Fig. 4 Simulation results. a Profile of the preplasma modeled by hydrodynamic simulation in terms of electron density N_e (density normalized to critical density N_c in the colorbar). The original target surface is located at $x = 0$ μm. The snapshot is captured at the moment of 14 ns after the prepulse arrival and the corresponding data are used as an input for the particle-in-cell simulation at the time 0 fs. **b** Transverse magnetic field B_z during the interaction of the peak laser intensity (main pulse) with the target modified by the picosecond prepulse, showing the incidence and reflection directions of the main pulse (in terms of normalized dimensionless field a_0) ~15 μm away from the original target surface. A contour of the preplasma having critical density depicted in black is added to the figure. **c** Energy distribution of simulated protons in the forward (into the target, red dashed line) and backward (away from the target, blue solid line) directions.

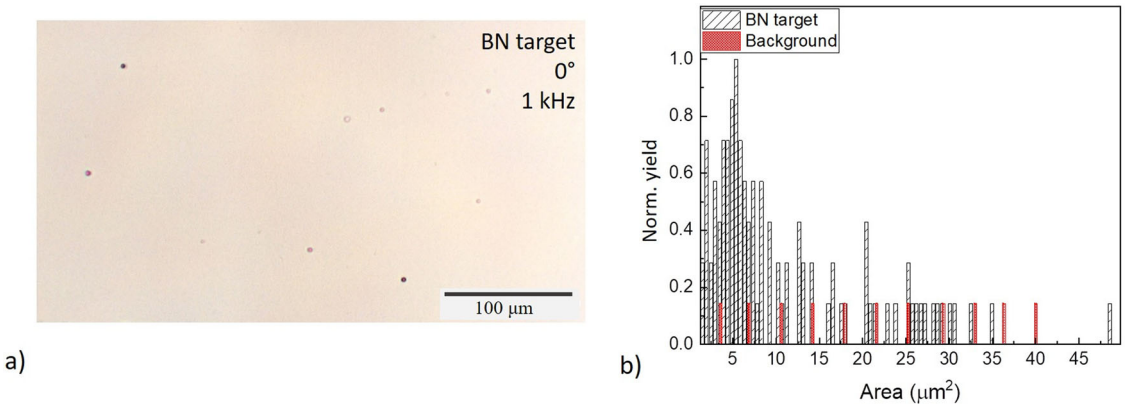

Fig. 5 Test at the kHz operation regime. a Example of the irradiated CR39 located at 0° of the filtered region (2.4 Al μm) after 3 h of etching and recorded at 1-kHz repetition rate using a BN target. **b** The area distribution of the recorded particle tracks for all the CR39 samples under conditions described in a).

experimental conditions. It is important to highlight that other experiments related to laser-driven alpha particles production via pB fusion have required high-energy, high-power laser facilities, which operate at very low repetition rates (e.g. one shot per 30 min at the PALS facility, as described in references[26,27]). On the other hand, implementation of kHz sources of laser-accelerated protons has recently been reported[39–42]. However, to the best of our knowledge, repetitive laser-driven alpha particle sources have never been demonstrated. Therefore, we have additionally carried out an effort to provide a proof-of-principle of the experimental generation of alpha particle beams at 1 kHz using a motorized target holder prototype designed for high-repetition-rate operation[43]. In such a test, a pure BN target was used with no plasma polymer layer deposited on it due to the target holder operation limitations, but taking advantage of adventitious hydrogen atoms present in the BN sample which were used as a source of protons. Figure 5a, b show raw CR39 data for a 0° filtered segment and area distribution of craters, respectively. Figure 5 proves the unambiguous generation of alpha particles achieved during the high-repetition rate run. Taking into account a very limited supply of protons from the BN target, it is not surprising that the overall alpha particle yield is small; however, it is evident that there is space for further optimization of the experimental conditions (e.g., target design and target holder optimization towards more efficient use of the kHz laser capability).

Discussion

A proof-of-concept experiment aimed at triggering laser-driven pB fusion reactions with a tabletop laser system was reported. Our approach combines the use of the secondary pB fusion cross-section resonance and a controlled prepulse to generate a hydrogen-boron preplasma at the target front side, which has led to the production of 6×10^4 alpha particles per second at 10 Hz and 10^6 alpha particles per second at 1 kHz. Despite the fact that previous successful campaigns were conducted at very large and complex state-of-the-art laser facilities (0.1–1 kJ, 0.01–1 PW), we have shown that laser-driven pB fusion is reachable also with ultra-compact and user-oriented laser systems operating at ~5 orders of magnitude lower laser pulse energies and peak powers (~10 mJ, ~10 GW).

The energy distribution of the generated alpha particles fell within the range expected from theory and previous experiments; however, it seemed to be slightly shifted towards lower energies with the spectrum peaked ~3.5 MeV. This might be ascribed to the Coulomb interaction of the alpha particles with the plasma plume while traveling towards the detectors. It is worth noting that opposed to our findings, previous works demonstrated enhancement in alpha particle energy due to the possible acceleration in the electric field of the plasma;[11,27] however, this was not recorded in our experiment because of the lower electric field present under the given different experimental conditions (moderate laser energy and intensity).

The experimental measurements were supported by a combination of HD and PIC numerical simulations, confirming the presence of protons accelerated to energies sufficient to exploit the secondary resonance peak in the reaction cross-section (148 keV, CoM). The numerical results suggest that, due to specific experimental conditions (~1.5-ps-long prepulse, $\sim 10^{-3}$ intensity contrast), the preplasma created prior to the main pulse arrival was strongly overdense. As a result, the main pulse was reflected by the preplasma (at the critical density surface) without reaching the target surface, and the main laser-matter interaction happened in the preplasma cloud. Moreover, simulations demonstrated that protons with energies up to 300 keV were accelerated backwards rather than towards the target. This implies that the pB fusion reaction was accessible only in the plasma region, where boron ions were present with a mean density of $\sim 5 \times 10^{19}/\mathrm{cm}^3$. Since the number of boron ions and protons in the preplasma was decreased in comparison to the initial solid target, this might elucidate the relatively low yield of measured alpha particles ($\sim 10^4$ particles/shot, i.e., $\sim 10^5$ particles/s at 10 Hz).

However, the relatively low number of alpha particles per shot can be compensated by entering the kHz operational regime, available with the PERLA B laser system, as it was preliminary realized during this experiment, thus reaching a repetitive source of multi-MeV (1–5 MeV) alpha particles with a current exceeding 10^6 particles/s. Such alpha particle currents can be further enhanced by using 100-mJ class lasers operating in the ps regime at 1 kHz (under development at the HiLASE center) that would allow exploring a similar laser-plasma interaction geometry in the intensity range of 10^{17}–$10^{18}\,\mathrm{W/cm}^2$. In such conditions, proton energies suitable for the main pB fusion cross-section resonance (~610 keV, CoM) could be achieved, hence implying a 100-fold (or higher) enhancement in the average alpha particle current (10^8–10^9 particles/s). Such values would be comparable with those obtained using high-intensity and high-energy PW-class lasers (e.g., as in ref. [28]).

Besides the PERLA system used for our experimental study, other ps-class laser systems operating at kHz and delivering up to 1 J energy in a single pulse have already been demonstrated[44], thus the alpha particle flux can be further enhanced by another order of magnitude and reach values $\sim 10^{10}$ per second. Additionally, the laser-target or laser-preplasma interaction can be optimized by target engineering (e.g., enhancing the overall hydrogen content) and prepulse control (both intensity contrast and delay time). This would allow a further enhancement of the alpha particle flux that could ultimately lead to $\sim 10^{11}$ per second. Such a value is of interest for the production of radioisotopes, nevertheless, other applications may require lower fluxes, e.g., non-destructive material investigation or nuclear reaction studies[22,45].

Methods

Laser and target setup. The experiment was performed at the HiLASE facility using the PERLA B laser, a compact system based on a thin-disk regenerative amplifier[30]. The PERLA laser is characterized by ~1.5 ps temporal duration, 1030 nm wavelength, and maximum laser energy up to 20 mJ (17 mJ at the output after the optical pathway in air) at 1 kHz repetition rate. The optical setup used in the experiment included (i) a half-wavelength plate to obtain p-polarization in order to efficiently couple laser energy to plasma electrons; (ii) a 6× beam expander enabling to improve of the laser intensity on target by minimizing the resulting focal spot; (iii) a f/2 focusing lens located inside the vacuum chamber; and iv) a protective glass placed in front of the focusing lens to protect it from the debris contamination. The measured laser intensity in the focal spot was $2.3 \times 10^{16}\,\mathrm{W/cm}^2$, with 37% of laser energy encircled within FWHM. A short (~1.5 ps) prepulse interacted with the target 14 ns prior to the main pulse, thus forming a preplasma. The contrast ratio between the intensity of the prepulse and the main pulse was 2.9×10^{-3}. The focusing lens was installed on a moving platform with micrometric movement, enabling to scan the focal position of the laser pulse on the target plane remotely.

The target was fixed onto a spiral target tower—a prototype of target handling systems aimed at high-repetition-rate operation, which by simultaneous rotational and translational motorized motions directs the laser shots so that a spiral shape is formed on the target surface[43]. The targets were stuck onto the rotating disk of the spiral tower. The target samples were always pre-aligned and checked using a monitoring system so that the surface coincided with the focal plane with an accuracy of <10 µm. The target flatness uncertainties were below the Rayleigh range of the focused beam (~15 µm).

The detectors (FC and CR39 described further) were located only in the backward direction since the target was too thick for particles to penetrate through it.

Faraday cup diagnostic. The Faraday cup (FC) that was used during the experiment is a conductive copper cup, biased at −100 V. The device is described in detail in ref. [35]. The current generated by the incoming charged particles is measured depending on time, resulting in a typical time-of-flight (TOF) spectrum.

The FC feedback was important during the experiment since it was the only online available ion diagnostic. First, it enabled to monitor of the laser-target interaction in real-time (shot-by-shot), thus ensuring timely detection of technical issues and also checking the stability of the laser-plasma interaction. Second, it was used to optimize the interaction by scanning the focal position of the laser at the beginning of the shot series for a given target by remotely changing the focusing lens position. As experimentally found and also predicted by simulations, the best focal position was slightly in front of the target surface, probably due to the preplasma cloud formation and its optimal interaction with the main laser pulse.

The average TOF signal together with the standard deviation for all the shots at the CH-BN target is shown in Fig. 6. The TOF spectra were relatively stable in terms of the start of the signal (maximum energy) and total flux. However, as outlined in the manuscript, the sensitivity of the FC was not high enough to measure the low number of the high-energy protons and alpha particles shot-by-shot. As demonstrated by the CR39 results, the total number of high-energy particles was around 10^3–10^4 particles/sr/shot, while the lower limit for the FC detection was $\sim 10^8$ particles/sr/shot (due to the noise level in the given experimental configuration).

Target production technique. The targets were produced specifically for this experiment using a method of plasma-assisted vapor phase deposition developed at the department of macromolecular physics at Charles University (Prague)[46,47]. A conventional poly(ethylene) sample is heated under 1 Pa Ar pressure to a temperature of 280 °C at which thermal decomposition of macromolecules occurs. The decomposition proceeds with the release of (CH2)100 oligomers into the gas[48]. The oligomer flux then passes through a zone of capacitively-coupled low-temperature plasma (rf, 13.56 MHz, 15 W) in which oligoethylenes become activated by electron impact with the formation of free radicals. The plasma-activated species arrive onto BN substrates (provided by FBK), where they recombine and form a thin film of a hydrocarbon plasma polymer. The cross-link density and the hydrogen content in the plasma polymer can be controlled by the power of the rf discharge and the evaporation rate. The method avoids the use of solvents and chemicals and allows for the deposition of thin films with thicknesses in the nm-to-µm range, which can be highly versatile for future experiments. For this proof-of-principle experiment, CH plasma polymer films with H/C ratio of 1.88 and thickness of 600 nm were deposited onto the 3-mm thick BN substrates. In such a configuration, the CH

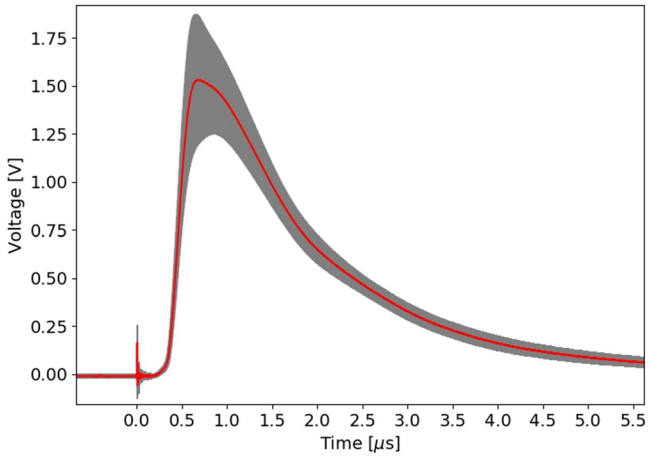

Fig. 6 Faraday cup measurements. Averaged TOF (time-of-flight) signal for all shots at the CH-BN target (red) together with standard deviation (gray). The beginning of the signal is very stable, while the flux fluctuates shot-by-shot.

plasma polymer serves as a source of hydrogen, whereas the BN substrate supplies the boron fuel.

CR39 nuclear-track diagnostics. In order to detect the produced alpha particles, two CR39 detectors[49,50] were located at the front side of the target in each experimental run. One was placed slightly above the equatorial plane and the other one below it to assure the detection of ions by the FC. To obtain the angular distribution of the alpha particles, the 20-cm long CR39 stripes were placed at a distance of 8 cm from the laser-target interaction point, thus enabling a maximum detection angle of ~68° (from −20° to +48°), considering the target normal as the reference axis (0°). The first stripe was left uncovered to detect all the ions (both from the plasma and the pB fusion reaction), while the second stripe was covered by a 2.4-μm thick Al filter. The use of the Al filter allowed to exclude the presence of protons with energies below ~300 keV but, at the same time, prevented to detect alpha particles with energies below ~700 keV. An unexposed (non-irradiated) CR39 stripe was used to measure the contribution of the natural background. The CR39s were etched in a solution of NaOH 6.25 M at 70 °C for 3 h and the revealed tracks were recorded by an optical microscope coupled to a CCD camera. The CR39 used in the experiment were calibrated with an alpha particle source as discussed elsewhere[28].

HD simulation. For the HD simulations, the 2D cylindrical FLASH[37,38] code using three temperatures (electron, ion, and radiation) and two fluids (electron and ion) was employed. The target was initialized as cold and semi-infinite. In the equation of state, the density of the polymer deposition on the boron base target was used as 0.93 g/cm^2. A laser prepulse of 50 μJ energy and 1.5 ps duration was incident onto the target obliquely at 45°, with FWHM of the beam on the target plane set as 6.95 μm (according to the experimental measurements described above). After the interaction, the matter was allowed to evolve for 14 ns, which is the time delay between the prepulse and the main pulse arrival. To prevent the natural expansion of a target in the FLASH code, a condition was put ensuring that the target could not evolve until it reached 1000 K, therefore, only the areas affected by the laser would expand.

PIC simulation. 2D PIC simulations were performed using the full-relativistic electromagnetic particle-in-cell code SMILEI[51]. Initial plasma conditions (electron and ion densities) around the original target surface were set based on the output of HD simulations, i.e., corresponding to the time of 14 ns after the prepulse arrival. Ionization of the CH target layer was set to $C^{4+}H^{+}$, the maximum electron density n_e was reduced to 10 n_{ec} at the numerical cells where $n_e > 10\ n_{ec}$, vacuum was assumed at the numerical cells where the electron density was below 0.002 n_{ec}, and the simulation area was modified due to computational constraints. The main laser pulse was incident onto the original target plane obliquely at 45°, the pulse duration was 1.5 ps at FWHM, and the temporal shape of the pulse was approximated by cos^2 intensity profile with full duration of 3.2 ps. The peak intensity of the laser pulse was set to 8×10^{16} W/cm^2 according to a focal spot width of 2.65 μm. The focal position was moved by 50 μm away from the target.

Output data from HD simulation (array of 800 × 750 numerical cells) specifying electron densities were firstly transformed into plasma density in 10240 × 5120 cells in PIC simulation. Here, the size of each cell was set to 8 × 8 nm^2. Compared to HD simulations, the simulation area of the PIC modeling was adjusted in order to cover only the main interaction region in order to spare computer memory and computational time. Then, numerical particles were randomly initialized based on plasma density in each cell. Numerical weights of each particle were set in order to have 20 electrons, 20 protons, and 10 C^{4+} ions per cell at maximum plasma density 10 n_{ec} and at least one numerical particle for each species per cell at minimum density 0.002 n_{ec}. Such setup led to a total number of 157×10^6 electrons and protons, and 89×10^6 C^{4+} ions in the simulation. Thermal boundary conditions were applied at the simulation box boundaries with an initial temperature of all particle species equal to 10 eV. A second-order shape function of numerical particles was used. The whole simulation consists of 210,000 time steps, calculating the evolution of plasma for 3.5 ps.

Data availability

Data are available upon reasonable request.

Code availability

The codes used to benchmark the experimental results (hydrodynamic and particle-in-cell codes are available upon reasonable request).

Received: 24 July 2022; Accepted: 13 January 2023;
Published online: 02 February 2023

References

1. Oliphant, M. L. E. & Rutherford, E. Experiments on the transmutation of elements by protons. *Proc. R. Soc. Lond. Ser. A* **141**, 259–281 (1933).
2. Quebert, J. & Marquez, L. Effets des résonances de 12C sur l'émission de particules alpha dans la réaction 11B (p, 3α). *Nucl. Phys. A* **126**, 646–670 (1969).
3. Moreau, D. C. Potentiality of the proton-boron fuel for controlled thermonuclear fusion. *Nucl. Fusion* **17**, 13 (1977).
4. Martinez-Val, J., Eliezer, S., Piera, M. & Velarde, G. Fusion burning waves in proton-boron-11 plasmas. *Phys. Lett. A* **216**, 142–152 (1996).
5. Nevins, W. M. & Swain, R. The thermonuclear fusion rate coefficient for p-11B reactions. *Nucl. fusion* **40**, 865 (2000).
6. Dmitriev, V. F. α-particle spectrum in the reaction p+ 11B→ α+ 8Be*→ 3α. *Phys. At. Nucl.* **72**, 1165–1167 (2009).
7. Becker, H. W., Rolfs, C. & Trautvetter, H. P. Low-energy cross sections for11B (p, 3α). *Z. für. Phys. A At. Nucl.* **327**, 341–355 (1987).
8. Spraker, M. C. et al. The 11B (p, α) 8Be→ α+ α and the 11B (α, α) 11B reactions at energies below 5.4 MeV. *J. Fusion Energy* **31**, 357–367 (2012).
9. Sikora, M. H. & Weller, H. R. A new evaluation of the 11B(P, α)αα reaction rates. *J. Fusion Energy* **35**, 538–543 (2016).
10. Stave, S. et al. Understanding the B11 (p, α) αα reaction at the 0.675 MeV resonance. *Phys. Lett. B* **696**, 26–29 (2011).
11. Margarone, D. et al. In-target proton–boron nuclear fusion using a PW-class laser. *Appl. Sci.* **12**, 1444 (2022).
12. Labaune, C. et al. Laser-initiated primary and secondary nuclear reactions in boron-nitride. *Sci. Rep.* **6**, 1–8 (2016).
13. Rostoker, N., Qerushi, A. & Binderbauer, M. Colliding beam fusion reactors. *J. Fusion Energy* **22**, 83–92 (2003).
14. Hora, H. et al. Fusion energy using avalanche increased boron reactions for block-ignition by ultrahigh power picosecond laser pulses. *Laser Part. Beams* **33**, 607–619 (2015).
15. Hora, H. et al. Road map to clean energy using laser beam ignition of boron-hydrogen fusion. *Laser Part. Beams* **35**, 730–740 (2017).
16. Yoon, D. K., Jung, J. Y. & Suh, T. S. Application of proton boron fusion reaction to radiation therapy: a Monte Carlo simulation study. *Appl. Phys. Lett.* **105**, 223507 (2014).
17. Giuffrida, L. et al. Prompt gamma ray diagnostics and enhanced hadron-therapy using neutron-free nuclear reactions. *AIP Adv.* **6**, 105204 (2016).
18. Cirrone, G. A. P. First experimental proof of Proton Boron Capture Therapy (PBCT) to enhance protontherapy effectiveness. *Sci. Rep.* **8**, 1–15 (2018).
19. Bláha, P. et al. The proton-boron reaction increases the radiobiological effectiveness of clinical low-and high-energy proton beams: novel experimental evidence and perspectives. *Front. Oncol.* **11**, 682647 (2021).
20. Petringa, G. et al. Prompt gamma-ray emission for future imaging applications in proton-boron fusion therapy. *J. Instrum.* **12**, C03059 (2017).
21. Petringa, G. et al. Study of gamma-ray emission by proton beam interaction with injected Boron atoms for future medical imaging applications. *J. Instrum.* **12**, C03049 (2017).
22. Qaim, S. M. et al. Uses of alpha particles, especially in nuclear reaction studies and medical radionuclide production. *Radiochim. Acta* **104**, 601–624 (2016).
23. Szkliniarz, K. et al. Production of medical Sc radioisotopes with an alpha particle beam. *Appl. Radiat. Isot.* **118**, 182–189 (2016).
24. Belyaev, V. S. et al. Observation of neutronless fusion reactions in picosecond laser plasmas. *Phys. Rev. E* **72**, 026406 (2005).
25. Labaune, C. et al. Fusion reactions initiated by laser-accelerated particle beams in a laser-produced plasma. *Nat. Commun.* **4**, 1–6 (2013).
26. Picciotto, A. et al. Boron-proton nuclear-fusion enhancement induced in boron-doped silicon targets by low-contrast pulsed laser". *Phys. Rev. X* **4**, 031030 (2014).
27. Giuffrida, L. et al. High-current stream of energetic α particles from laser-driven proton-boron fusion. *Phys. Rev. E* **101**, 013204 (2020).
28. Margarone, D. et al. Generation of α-particle beams with a multi-kJ, Peta-Watt class laser system. *Front. Phys.* **8**, 343 (2020).
29. Bonvalet, J. Energetic α-particle sources produced through proton-boron reactions by high-energy high-intensity laser beams. *Phys. Rev. E* **103**, 053202 (2021).
30. Smrž, M. et al. Advances in High-Power, Ultrashort Pulse DPSSL Technologies at HiLASE. *Appl. Sci.* **7**, 1016 (2017).
31. McKenna, P. et al. Effects of front surface plasma expansion on proton acceleration in ultraintense laser irradiation of foil targets. *Laser Part. Beam* **26**, 591–596 (2008).
32. Passoni, M., Tikhonchuk, V., Lontano, M. & Bychenkov, V. Y. Charge separation effects in solid targets and ion acceleration with a two-temperature electron distribution. *Phys. Rev. E* **69**, 026411 (2004).
33. Margarone, D. et al. High current, high energy proton beams accelerated by a subnanosecond laser. *Nucl. Instrum. Methods Phys. Res. Sect. A* **563**, 159–163 (2011).

34. Prokůpek, J. et al. Development and first experimental tests of Faraday cup array. *Rev. Sci. Instrum.* **85**, 013302 (2014).
35. Margarone, D. et al. Full characterization of laser-accelerated ion beams using Faraday cup, silicon carbide, and single-crystal diamond detectors. *J. Appl. Phys.* **109**, 103302 (2011).
36. Davidson, J. M. et al. Low energy cross sections for 11B (p, 3α). *Nucl. Phys. A.* **315**, 253–268 (1979).
37. Fryxell, B. et al. FLASH: an adaptive mesh hydrodynamics code for modeling astrophysical thermonuclear flashes. *Astrophys. J.* **131**, 273 (2000).
38. Dubey, A. et al. Extensible component-based architecture for FLASH, a massively parallel, multiphysics simulation code. *Parallel Comput.* **35**, 512–522 (2009).
39. Singh, P. K. et al. Low divergent MeV-class proton beam with micrometer source size driven by a few-cycle laser pulse. *Sci. Rep.* **12**, 8100 (2022).
40. Hou, B. et al. MeV proton beams generated by 3 mJ ultrafast laser pulses at 0.5 kHz". *Appl. Phys. Lett.* **95**, 101503 (2009).
41. Morrison, J. T. et al. MeV proton acceleration at kHz repetition rate from ultra-intense laser liquid interaction". *N. J. Phys.* **20**, 022001 (2018).
42. Levy, D. et al. Low-divergence MeV-class proton beams from kHz-driven laser–solid interactions. *Phys. Rev. Acc. Beams* **25**, 093402 (2022).
43. Chagovets, T. et al. Automation of target delivery and diagnostic systems for high repetition rate laser-plasma acceleration. *Appl. Sci.* **11**, 1680 (2021).
44. Wang, Y. et al. 1.1 J Yb: YAG picosecond laser at 1 kHz repetition rate". *Opt. Lett.* **45**, 6615–6618 (2020).
45. Pappalardo, L. et al. The improved LNS PIXE-alpha portable system: archaeometric applications.". *Archaeometry* **45**, 333–339 (2003).
46. Choukourov, A. et al. Microphase-separated PE/PEO thin films prepared by plasma-assisted vapor phase deposition. *ACS Appl. Mater. Interfaces* **8**, 8201–8212 (2016).
47. Choukourov, A. et al. Plasma-assisted growth of polyethylene fractal nano-islands on polyethylene oxide films: impact of film confinement and glassy dynamics on fractal morphologies. *Appl. Surf. Sci.* **489**, 55–65 (2019).
48. Choukourov, A. et al. Self-organization of vapor-deposited polyolefins at the solid/vacuum interface. *Prog. Org. Coat.* **143**, 105630 (2020).
49. Cartwright, B. G., Shirk, E. & Price, P. A nuclear-track-recording polymer of unique sensitivity and resolution. *Nucl. Instrum. Methods* **153**, 457–460 (1978).
50. Azooz, A. A. & Al-Jubbori, M. A. Alpha particles energy estimation from track diameter development in a CR-39 detector. *Appl. Radiat. Isot.* **115**, 74–80 (2016).
51. Deroullait, J. et al. Smilei: A collaborative, open-source, multi-purpose particle-in-cell code for plasma simulation. *Comput. Phys. Commun.* **222**, 351 (2018).

Acknowledgements

This research was funded by the Ministry of Education, Youth, and Sports of the Czech Republic through the project "Advanced Research Using High-Intensity Laser-Produced Photons and Particles" (CZ.02.1.010.00.016_0190000789), the European Union's Horizon 2020 research and innovation program (Grant agreement no. 871124, LASERLAB-EUROPE), the project "Target Engineering for Proton-Boron Nuclear Fusion Studies" sponsored by the UK Royal Society, and the EUROfusion Consortium, which was funded by the European Union via the Euratom Research and Training Program (Grant agreement no. 101052200—EUROfusion). This work has been partly supported by project 18HLT04 UHDpulse, which has received funding from the EMPIR programme cofinanced by the Participating States and from the European Union's Horizon 2020. Computational resources for PIC simulations (Hyperion cluster at Czech Technical University) were funded by the European Regional Development Fund—Project "Centre of Advanced Applied Sciences" (no. CZ.02.1.01/0.0/0.0/16_019/0000778). The FLASH code was developed by the DOE NNSA-ASC OASCR Flash Center at the University of Chicago. Y.L. acknowledges the support from the European Regional Development Fund and the state budget of the Czech Republic (project BIATRI: no. CZ.02.1.01/0.0/0.0/15_003/0000445). M.T. acknowledges the support of Charles University through the student grant SVV 260 579-2021.

Author contributions

The paper's initial idea was proposed by D.M., L.G., A.L.; the experiment was organized by D.M., L.G., T.M., S.K., M.B.; the experiment was carried out by V.I., M.T., F.G., V.K., S.S., A.H., Y.L., J.H., M.C.; the data analysis was performed by V.I., M.T., S.D.S., V.K., A.H., F.B.; the hydrodynamic simulations were carried out by A.M., the P.I.C. simulations were carried out by J.P.; the target fabrication was performed by M.T., P.P., D.N., A.C., A.P.; the original draft was prepared by V.I. and D.M., and the review and editing were performed by all authors. All authors have read and agreed to the published version of the manuscript.

Competing interests

The authors declare no competing interests. Daniele Margarone is an Editorial Board Member for Communications Physics, but was not involved in the editorial review of, or the decision to publish this article.

Additional information

Supplementary information The online version contains supplementary material available at https://doi.org/10.1038/s42005-023-01135-x.

Correspondence and requests for materials should be addressed to Valeriia Istokskaia or Daniele Margarone.

Peer review information *Communications Physics* thanks Karoly Osvay and the other, anonymous, reviewers for their contribution to the peer review of this work. Peer reviewer reports are available.

Reprints and permission information is available at http://www.nature.com/reprints

Publisher's note Springer Nature remains neutral with regard to jurisdictional claims in published maps and institutional affiliations.